

# ULRR

## Pillar modularity in fsc topology hybrid ultramicroporous materials based upon tetra(4-pyridyl)benzene

Item Type	Article
Authors	Sensharma, Debobroto;Wilson, Ben;Kumar, Naveen;O'Hearn, Daniel;Zaworotko, Michael
Citation	Crystal Growth and Design, 2022, 22, (9), pp. 5472–5480
Publisher	American Chemical Society
Download date	2026-06-16 18:53:15
Item License	<a href="https://creativecommons.org/licenses/by-nc-sa/4.0/">https://creativecommons.org/licenses/by-nc-sa/4.0/</a>
Link to Item	<a href="https://doi.org/10.34961/researchrepository-ul.24290923">https://doi.org/10.34961/researchrepository-ul.24290923</a>

# Pillar Modularity in fsc Topology Hybrid Ultramicroporous Materials Based upon Tetra(4-pyridyl)benzene

Debobroto Sensharma,<sup>#</sup> Benjamin H. Wilson,<sup>#</sup> Naveen Kumar, Daniel J. O'Hearn, and Michael J. Zaworotko\*



Cite This: <https://doi.org/10.1021/acs.cgd.2c00561>



Read Online

ACCESS |



Metrics & More

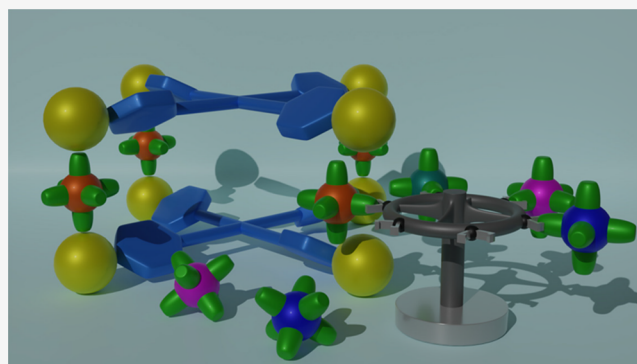


Article Recommendations



Supporting Information

**ABSTRACT:** Hybrid ultramicroporous materials (HUMs) are porous coordination networks composed of combinations of organic and inorganic linker ligands with a pore diameter of <7 Å. Despite their benchmark gas sorption selectivity for several industrially relevant gas separations and their inherent modularity, the structural and compositional diversity of HUMs remains underexplored. In this contribution, we report a family of six HUMs (SIFSIX-22-Zn, TIFSIX-6-Zn, SNFSIX-2-Zn, GEFSIX-4-Zn, ZRFSIX-3-Zn, and TAFSEVEN-1-Zn) based on Zn metal centers and the tetratopic N-donor organic ligand tetra(4-pyridyl)benzene (tepb). The incorporation of fluorinated inorganic pillars (SiF<sub>6</sub><sup>2-</sup>, TiF<sub>6</sub><sup>2-</sup>, SnF<sub>6</sub><sup>2-</sup>, GeF<sub>6</sub><sup>2-</sup>, ZrF<sub>6</sub><sup>2-</sup>, and TaF<sub>7</sub><sup>2-</sup>, respectively) resulted in (4,6)-connected fsc topology as verified using single-crystal X-ray diffraction. Pure-component gas sorption studies with N<sub>2</sub>, CO<sub>2</sub>, C<sub>2</sub>H<sub>2</sub>, C<sub>2</sub>H<sub>4</sub>, and C<sub>2</sub>H<sub>6</sub> revealed that the large voids and narrow pore windows common to all six HUMs can be leveraged to afford high C<sub>2</sub>H<sub>2</sub> uptakes while retaining high ideal adsorbed solution theory (IAST) selectivities for industrially relevant gas mixtures: >10 for 1:99 C<sub>2</sub>H<sub>2</sub>/C<sub>2</sub>H<sub>4</sub> and >5 for 1:1 C<sub>2</sub>H<sub>2</sub>/CO<sub>2</sub>. The approach taken, systematic variation of pillars with retention of structure, enables differences in selectivity to be attributed directly to the choice of the inorganic pillar. This study introduces fsc topology HUMs as a modular platform that is amenable to fine-tuning of structure and properties.



## INTRODUCTION

[Zn(4,4'-bipyridine)<sub>2</sub>(SiF<sub>6</sub>)<sub>n</sub>] (SIFSIX-1-Zn), reported in 1995,<sup>1</sup> is the prototypal hybrid coordination network (HCN) and is the parent of what is today a broad and growing platform of porous materials with a diverse range of topologies, pore sizes, pore chemistries, and properties.<sup>2</sup> That both the pore size and pore chemistry of HCNs are amenable to fine-tuning through crystal engineering approaches is a consequence of their inherently modular nature, which comes from their typical compositions: a divalent metal ion node, neutral N-donor linker ligand, and inorganic anion pillar.<sup>2</sup> The resulting hybrid coordination networks are thereby composed of geometrically simple components.<sup>3</sup> The ready availability of N-donor linker ligands of varying lengths (e.g., pyrazine, 2.8 Å; 4,4'-bipyridine, 7.1 Å; N,N'-di(4-pyridyl)-1,4,5,8-naphthalenediimide, 15.4 Å) and inorganic dianions that can serve as linkers that offer strong electrostatics (e.g., SiF<sub>6</sub><sup>2-</sup>, GeF<sub>6</sub><sup>2-</sup>, AlF<sub>5</sub><sup>2-</sup>, NbOF<sub>5</sub><sup>2-</sup>, MoO<sub>4</sub><sup>2-</sup>, Cr<sub>2</sub>O<sub>7</sub><sup>2-</sup>) has been exploited to fine-tune properties that are of relevance to several important industrial separation challenges.<sup>4–11</sup> In particular, HCNs with pore diameters <7 Å (hybrid ultramicroporous materials, HUMs) exhibit selectivity values that are in some cases orders of magnitude greater than previous benchmark porous

materials: SIFSIX-18-Ni-β, NbOFFIVE-1-Ni, and TIFSIX-3-Ni for direct air capture of CO<sub>2</sub>; SIFSIX-14-Cu-i for removal of acetylene from ethylene; and CROFOUR-1-Ni for Xe/Kr separation.<sup>12–22</sup>

Although crystal engineering has enabled systematic access to platforms of HUMs with exceptional properties, there is limited topological diversity among the HUMs reported thus far. The majority of HCNs, including HUMs, are pcu topology nets composed of octahedral metal centers linked by two ditopic N-donor linker ligands and a ditopic inorganic pillar anion. Among the non-pcu topology HCNs, only those that exhibit mmo topology have been studied systematically.<sup>23</sup> Prior to the recent reports of ZJU-280 (SIFSIX-22-Cu, [Cu(tepb)SiF<sub>6</sub>]) and TIFSIX-Cu-TPB (TIFSIX-6-Cu, [Cu(tepb)TiF<sub>6</sub>]), fsc-2-SIFSIX ([Cu<sub>3</sub>(4-(pyridin-4-yl)acrylic acid)<sub>4</sub>(SiF<sub>6</sub>)]), CPM-131 ([[(TPyP-Fe)Zn(SiF<sub>6</sub>)]]), and its

Received: May 17, 2022

Revised: August 9, 2022

analogues ( $[(\text{TPyP-M})\text{Cu}(\text{NbOF}_5)]$ ,  $M = \text{Zn, Fe, Ni}$ ) were the only HCNs with (4,6)-connected **fsc** topology, and their sorption properties were found to be driven by coordinatively unsaturated metal centers (UMCs) rather than electrostatics and tight binding sites.<sup>24–28</sup> In **fsc-2-SIFSIX**, a bifunctional organic linker ligand allows for incorporation of both mononuclear Cu(II) and dinuclear  $\{\text{Cu}_2\}$  paddle-wheel building blocks into the final structure.<sup>28</sup> **CPM-131** (and the related **fsx** net **CPM-132**) is constructed using a porphyrin-based metalloligand, and despite the challenges of tuning a porphyrin-based system, it exemplifies HCNs based on a polytopic (used herein to refer to connectivity  $>2$ ) ligand.<sup>25,26</sup> In 2016, Lusi *et al.* reported a family of HCNs based on the polytopic linker Tripp (2,4,6-tris(4-pyridyl)pyridine), **Tripp-Cu-MFSIX** ( $[[\text{Cu}_6(\text{Tripp})_8](\text{MF}_6)_3(\text{MF}_6)_3]$ ).<sup>29</sup> These structures formed a partially bridged **pto**-type net but were not found to be permanently porous despite large solvent-accessible voids. A notable feature of this platform is that five distinct inorganic pillar dianions were incorporated into the same structure. More recently, Wu *et al.* reported an **ith-d** topology framework, **SIFSIX-Cu-TPA** ( $[\text{Cu}_3(\text{TPA})_4(\text{SiF}_6)_3]$ ), using a tritopic linker ligand, TPA (tri(pyridin-4-yl)amine).<sup>30</sup> Our group recently reported the **fsc** frameworks **SIFSIX-22-Zn** and **SOFOUR-1-Zn**, both of which are based on the **tepb** linker.<sup>31</sup>

The modularity of a porous coordination network (PCN) can be expressed in terms of how many components can be varied independently. HCNs based on two-dimensional nets pillared by MFSIX to form **pcu** networks are highly modular, having three components that can be varied independently (organic linker ligand, inorganic anionic pillar ligand, and metal cation node).<sup>2</sup> Additionally, there are cases in which interpenetration can also be controlled, for example, in **SIFSIX-2-Cu** and **SIFSIX-2-Cu-i**.<sup>4</sup> The resulting drastic effect on the pore size and pore chemistry that results from interpenetration (and therefore properties) offers a fourth variable by which such a platform can be modulated. This level of modularity (four components) is only met or surpassed by platforms that combine mixed linkers and/or extra-framework anions/cations. Most other well-known PCNs, such as those based on oxo-clusters and carboxylate linkers, offer just one or two modular components, limiting the scope of related materials that can be generated and, therefore, the extent to which properties can be “fine-tuned”.

A crystal engineering approach predominantly based on ditopic linker ligands means that most HCNs exhibit nearly cylindrical one-dimensional channels with a high density of tight binding sites to drive their sorption properties. The design of HCNs based on polytopic ligands offers the possibility of new types of channel architectures and new structure–property relationships. In their recent work on **ZJU-280** (**SIFSIX-22-Cu**), Qian and co-workers reported a HUM that is composed of a tetratopic linker ligand in place of the more commonly used ditopic linkers, presenting an opportunity for the development of a new HUM platform for the study of structure–property relationships.<sup>24</sup> We recently reported **SIFSIX-22-Zn** and **SOFOUR-1-Zn** using the same tetrapyrrolyl linker and  $\text{SiF}_6^{2-}$  or  $\text{SO}_4^{2-}$  pillars, respectively.<sup>31</sup> In the present work, we report a crystal engineering study of **fsc** HUMs involving substitution of the inorganic pillars in  $[\text{Zn}(\text{tepb})\text{SiF}_6]$  (**SIFSIX-22-Zn**) to afford an additional five members of this platform:  $[\text{Zn}(\text{tepb})\text{TiF}_6]$  (**TIFSIX-6-Zn**),  $[\text{Zn}(\text{tepb})\text{SnF}_6]$  (**SNFSIX-2-Zn**),  $[\text{Zn}(\text{tepb})\text{GeF}_6]$  (**GEFSIX-**

**4-Zn**),  $[\text{Zn}(\text{tepb})\text{ZrF}_6]$  (**ZRFSIX-3-Zn**), and  $[\text{Zn}(\text{tepb})\text{TaF}_7]$  (**TAFSEVEN-1-Zn**).

## EXPERIMENTAL SECTION

**Materials and Methods.** All reagents and solvents were used as received from vendors. <sup>1</sup>H NMR spectroscopy was performed using a JEOL ECX400 spectrometer operating at 400 MHz. Thermal gravimetric analysis (TGA) was performed using a TA Q50 analyzer with a ramp rate of 10.00 °C/min from 25 to 500 °C and nitrogen gas flow of 40 mL/min. Powder X-ray diffraction (PXRD) diffractograms were recorded using a PANalytical X'Pert operated at 40 kV and 40 mA and  $\text{CuK}_\alpha$  radiation ( $\lambda_\alpha = 1.540598 \text{ \AA}$ ) was used for diffraction experiments. Incident beam optics included the Fixed Divergence slit with antiscatter slit PreFLX module, with a  $1/8^\circ$  divergence slit and a  $1/4^\circ$  antiscatter slit, as well as a 10 mm fixed incident beam mask and a Ni- $\beta$  filter. Data were collected from  $5^\circ$ – $40^\circ$  ( $2\theta$ ) with a step-size of  $0.0131303^\circ$  and a scan time of 30 s per step.

**Synthesis of 1,2,4,5-Tetra(4-pyridyl)benzene, **tepb**.** 1,2,4,5-Tetra(4-pyridyl)benzene (**tepb**) was synthesized according to the procedure reported by Chang and Wang.<sup>32</sup>  $\text{Fe}(\text{NO}_3)_3 \cdot 9\text{H}_2\text{O}$  (0.161 g, 0.4 mmol),  $\text{H}_3\text{PO}_4$  (0.6 mL, 9 mmol), 1,3-bis(4-pyridyl)propane (1.268 g, 6.4 mmol), oxalic acid dihydrate (0.151 g, 1.2 mmol), and water (2 mL) were combined in a Teflon-lined pressure vessel and heated at 180 °C for 48 h. Needle crystals of **tepb** were manually removed, washed with cold methanol, and dried (yield: ca. 50%). <sup>1</sup>H NMR (400 MHz,  $\text{DMSO-d}_6$ ):  $\delta = 8.48$  (8H, d), 7.61 (2H, s), 7.24 (8H, d).

**Synthesis of  $[\text{Zn}(\text{tepb})\text{SiF}_6]$ , **SIFSIX-22-Zn.** A solution of  $\text{ZnSiF}_6 \cdot 6\text{H}_2\text{O}$  (1.0 mg, 0.003 mmol) in 0.4 mL of methanol was put in a narrow glass tube. Methanol (0.2 mL) was carefully layered over this solution to act as a buffer layer before a solution of **tepb** (1.2 mg, 0.003 mmol) in 0.4 mL methanol was layered over the buffer layer. The tube was left undisturbed for 5 days, at which point colorless block crystals of  $[\text{Zn}(\text{tepb})\text{SiF}_6] \cdot x\text{MeOH}$  (as-synthesized **SIFSIX-22-Zn**) were obtained. A larger quantity of **SIFSIX-22-Zn** was prepared as follows:  $\text{ZnSiF}_6 \cdot 6\text{H}_2\text{O}$  (41.2 mg, 0.13 mmol) was added to a solution of **tepb** (77.2 mg, 0.20 mmol) in 16 mL methanol and stirred at room temperature overnight.  $[\text{Zn}(\text{tepb})\text{SiF}_6] \cdot x\text{MeOH}$  was obtained as a white microcrystalline powder which was isolated by filtration before being washed with methanol and air dried. Yield: 43.0 mg, 56%. CHN analysis calculated for  $\text{C}_{26}\text{H}_{26}\text{F}_6\text{N}_4\text{O}_4\text{SiZn}$  (including four interstitial water molecules): C 46.89%, H 3.94%, N 8.41%; experimental: C 46.72%, H 3.12%, N 8.27%.**

**Synthesis of  $[\text{Zn}(\text{tepb})\text{TiF}_6]$ , **TIFSIX-6-Zn.** A solution of  $\text{Zn}(\text{NO}_3)_2 \cdot 6\text{H}_2\text{O}$  (0.89 mg, 0.003 mmol) and  $(\text{NH}_4)_2\text{TiF}_6$  (0.59 mg, 0.003 mmol) in 0.2 mL of water was placed in a narrow glass tube. 1:1 methanol/water (0.4 mL) was carefully layered over this solution to act as a buffer layer before a solution of **tepb** (1.2 mg, 0.003 mmol) in 0.4 mL methanol was layered over the buffer layer, and the tube was left undisturbed for 3 days, at which point colorless block crystals of  $[\text{Zn}(\text{tepb})\text{TiF}_6] \cdot x\text{MeOH}$  (as-synthesized **TIFSIX-6-Zn**) were obtained. A bulk sample of **TIFSIX-6-Zn** was prepared as follows:  $\text{Zn}(\text{NO}_3)_2 \cdot 6\text{H}_2\text{O}$  (77.3 mg, 0.26 mmol) and  $(\text{NH}_4)_2\text{TiF}_6$  (51.5 mg, 0.26 mmol) in 1.0 mL of water was added to a solution of **tepb** (154.4 mg, 0.4 mmol) in 30 mL methanol and stirred at room temperature overnight.  $[\text{Zn}(\text{tepb})\text{TiF}_6] \cdot x\text{MeOH}$  was obtained as a white microcrystalline powder, isolated by filtration, washed with methanol, and air-dried. Yield: 96 mg, 60%. CHN analysis calculated for  $\text{C}_{26}\text{H}_{28}\text{F}_6\text{N}_4\text{O}_5\text{TiZn}$  (including five interstitial water molecules): C 44.37%, H 4.01%, N 7.96%; experimental: C 44.37%, H 3.41%, N 8.11%.**

**Synthesis of  $[\text{Zn}(\text{tepb})\text{GeF}_6]$ , **GEFSIX-4-Zn.** A solution of  $\text{Zn}(\text{NO}_3)_2 \cdot 6\text{H}_2\text{O}$  (0.89 mg, 0.003 mmol) and  $(\text{NH}_4)_2\text{GeF}_6$  (0.66 mg, 0.003 mmol) in 0.2 mL of water was placed in a narrow glass tube. 1:1 methanol/water (0.4 mL) was carefully layered over this solution to act as a buffer layer. Finally, a solution of **tepb** (1.2 mg, 0.003 mmol) in 0.4 mL methanol was layered over the buffer layer, and the tube was left undisturbed for 3 days. Colorless block crystals of  $[\text{Zn}(\text{tepb})\text{GeF}_6] \cdot x\text{MeOH}$  (as-synthesized **GEFSIX-4-Zn**) were there-**

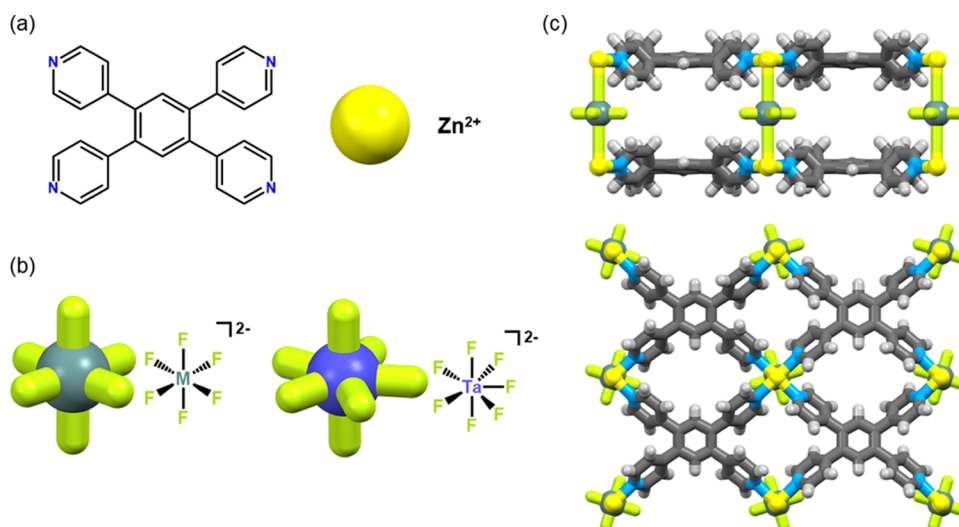


**Figure 1.** Representations of (a) tetra(4-pyridyl)benzene (tepb) ligand and Zn<sup>2+</sup> metal center; (b) MFSIX and TAFSEVEN pillars; and (c) fsc network [Zn(tepb)MF<sub>6</sub>] viewed along the *c* (above) and *a* (below) crystallographic axes.

by obtained. A bulk sample of GEFSEX-4-Zn was prepared as follows: Zn(NO<sub>3</sub>)<sub>2</sub>·6H<sub>2</sub>O (77.3 mg, 0.26 mmol) and (NH<sub>4</sub>)<sub>2</sub>GeF<sub>6</sub> (57.9 mg, 0.26 mmol) in 1.0 mL of water was added to a solution of **tepb** (154.4 mg, 0.4 mmol) in 30 mL methanol and stirred at room temperature overnight. [Zn(tepb)GeF<sub>6</sub>]*x*MeOH was obtained as a white microcrystalline powder, which was isolated by filtration, washed with methanol, and air-dried. Yield: 108 mg, 65%. CHN analysis calculated for C<sub>26</sub>H<sub>26</sub>F<sub>6</sub>N<sub>4</sub>O<sub>4</sub>GeZn (including four interstitial water molecules): C 43.95%, H 3.69%, N 7.87%; experimental: C 43.95%, H 3.24%, N 7.89%.

**Synthesis of [Zn(tepb)SnF<sub>6</sub>], SNFSIX-2-Zn.** A solution of Zn(NO<sub>3</sub>)<sub>2</sub>·6H<sub>2</sub>O (0.89 mg, 0.003 mmol) and (NH<sub>4</sub>)<sub>2</sub>SnF<sub>6</sub> (0.80 mg, 0.003 mmol) in 0.2 mL of water was placed in a narrow glass tube. 1:1 methanol/water (0.4 mL) was carefully layered over this solution to act as a buffer layer. Finally, a solution of **tepb** (1.2 mg, 0.003 mmol) in 0.4 mL methanol was layered over the buffer layer, and the tube was left undisturbed for 3 days. Colorless block crystals of [Zn(tepb)SnF<sub>6</sub>]*x*MeOH (as-synthesized SNFSIX-2-Zn) were thereby obtained. A bulk sample of SNFSIX-2-Zn was prepared as follows: a solution Zn(NO<sub>3</sub>)<sub>2</sub>·6H<sub>2</sub>O (77.3 mg, 0.26 mmol) and (NH<sub>4</sub>)<sub>2</sub>SnF<sub>6</sub> (69.4 mg, 0.26 mmol) in 1.0 mL of water was added to a solution of **tepb** (154.4 mg, 0.4 mmol) in 30 mL methanol and stirred at room temperature overnight. [Zn(tepb)SnF<sub>6</sub>]*x*MeOH was obtained as a white microcrystalline powder, which was isolated by filtration, washed with methanol, and air-dried. Yield: 119 mg, 67%. CHN analysis calculated for C<sub>26</sub>H<sub>34</sub>F<sub>6</sub>N<sub>4</sub>O<sub>8</sub>SnZn (including eight interstitial water molecules): C 37.69%, H 4.14%, N 6.76%; experimental: C 37.57%, H 3.20%, N 6.75%.

**Synthesis of [Zn(tepb)ZrF<sub>6</sub>], ZRFSIX-3-Zn.** A solution of Zn(NO<sub>3</sub>)<sub>2</sub>·6H<sub>2</sub>O (0.89 mg, 0.003 mmol) and K<sub>2</sub>ZrF<sub>6</sub> (0.85 mg, 0.003 mmol) in 0.2 mL of water was placed in a narrow glass tube. 1:1 methanol/water (0.4 mL) was carefully layered over this solution to act as a buffer layer. Finally, a solution of **tepb** (1.2 mg, 0.003 mmol) in 0.4 mL methanol was layered over the buffer layer, and the tube was left undisturbed for 3 days. Colorless block crystals of [Zn(tepb)ZrF<sub>6</sub>]*x*MeOH (as-synthesized ZRFSIX-3-Zn) were thereby obtained. A bulk sample of ZRFSIX-3-Zn was prepared as follows: A solution Zn(NO<sub>3</sub>)<sub>2</sub>·6H<sub>2</sub>O (77.3 mg, 0.26 mmol) and K<sub>2</sub>ZrF<sub>6</sub> (73.7 mg, 0.26 mmol) in 10.0 mL of water was added to a solution of **tepb** (154.4 mg, 0.4 mmol) in 30 mL methanol and stirred at room temperature overnight. [Zn(tepb)ZrF<sub>6</sub>]*x*MeOH was obtained as a white microcrystalline powder, which was isolated by filtration, washed with methanol, and air-dried. Yield: 116 mg, 68%. CHN analysis calculated for C<sub>26</sub>H<sub>28</sub>F<sub>6</sub>N<sub>4</sub>O<sub>5</sub>ZrZn (including five interstitial water molecules): C 41.80%, H 3.78%, N 7.50%; experimental: C 41.92%, H 2.91%, N 7.82%.

**Synthesis of [Zn(tepb)TaF<sub>7</sub>], TAFSEVEN-1-Zn.** A solution of Zn(NO<sub>3</sub>)<sub>2</sub>·6H<sub>2</sub>O (0.89 mg, 0.003 mmol) and (NH<sub>4</sub>)<sub>2</sub>TaF<sub>7</sub> (1.05 mg, 0.003 mmol) in 0.2 mL of water was placed in a narrow glass tube. 1:1 methanol/water (0.4 mL) was carefully layered over this solution to act as a buffer layer. Finally, a solution of **tepb** (1.2 mg, 0.003 mmol) in 0.4 mL methanol was layered over the buffer layer, and the tube was left undisturbed for 3 days. Colorless block crystals of [Zn(tepb)TaF<sub>7</sub>]*x*MeOH (as-synthesized TAFSEVEN-1-Zn) were thereby obtained. A bulk sample of TAFSEVEN-1-Zn was prepared as follows: a solution Zn(NO<sub>3</sub>)<sub>2</sub>·6H<sub>2</sub>O (77.3 mg, 0.26 mmol) and (NH<sub>4</sub>)<sub>2</sub>TaF<sub>7</sub> (91.0 mg, 0.26 mmol) in 1 mL of water was added to a solution of **tepb** (154.4 mg, 0.4 mmol) in 30 mL methanol and stirred at room temperature overnight. [Zn(tepb)TaF<sub>7</sub>]*x*MeOH was obtained as a white microcrystalline powder, which was isolated by filtration, washed with methanol, and air-dried. Yield: 113 mg, 57%. CHN analysis calculated for C<sub>26</sub>H<sub>22</sub>F<sub>6</sub>N<sub>4</sub>O<sub>2</sub>TaZn (including two interstitial water molecules): C 38.95%, H 2.77%, N 6.99%; experimental: C 38.81%, H 2.25%, N 7.05%.

**X-ray Crystallography.** Single-crystal X-ray crystallographic data were collected at 298 K on a Bruker D8 Quest diffractometer equipped with a CuK $\alpha$  microfocus source ( $\lambda = 1.5406 \text{ \AA}$ ) and Photon 100 detector. Temperature was controlled using a nitrogen flow from Oxford Cryosystems. Data was indexed, integrated and scaled in APEX3.<sup>33</sup> Absorption correction was performed by the multi-scan method using SADABS.<sup>34</sup> Space group determination was performed simultaneously with structure solution using the intrinsic phasing method (SHELXT),<sup>35</sup> and the solution was refined on F<sup>2</sup> using SHELXL<sup>36</sup> nonlinear least squares implemented in Olex2 v1.2.10.<sup>37</sup> All nonhydrogen atoms were refined anisotropically and hydrogen atoms bonded to carbon atoms were added at calculated positions and refined using a riding model. Disordered solvents were found in the cavity of all structures. Some of this electron density could be modeled as methanol molecules with partial occupancy; however, refinement was unsatisfactory, and the solvent atomic displacement parameters were unreasonable. The PLATON SQUEEZE<sup>38</sup> routine was performed to account for the electron density of unmodelled solvents, resulting in a more satisfactory refinement. The crystal structure CIF files have been deposited in the Cambridge Crystallographic Data Centre (CCDC: 2151309–2151313).

**Gas Sorption Measurements.** For gas sorption experiments, ultra-high purity gases were used as received from BOC Gases Ireland: He (99.999%), CO<sub>2</sub> (99.995%), C<sub>2</sub>H<sub>2</sub> (98.5%), N<sub>2</sub> (99.998%), C<sub>2</sub>H<sub>4</sub> (99.92%), and C<sub>2</sub>H<sub>6</sub> (99.0%). Adsorption isotherm experiments (up to 1 bar) for 195 K CO<sub>2</sub> were performed on a Micromeritics Tristar II 3030. A Micromeritics 3Flex surface area and pore size analyzer 3500 was used for collecting the 273 and 298 K

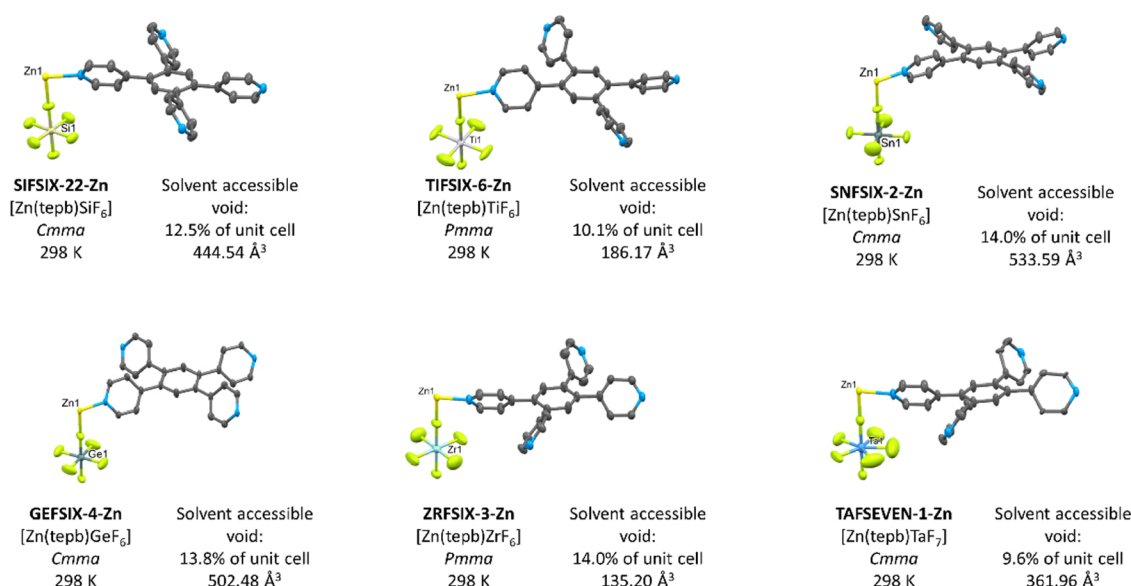


**Figure 2.** Formula units in SIFSIX-22-Zn, TIFSIX-6-Zn, SNFSIX-2-Zn, GEFSIX-4-Zn, ZRFSIX-3-Zn, and TAFSEVEN-1-Zn. Thermal ellipsoids are shown at a probability level of 50%.

sorption isotherms for all gases. The low temperature of 195 K was maintained using a dry ice-acetone mixture. Bath temperatures of 273 and 298 K were precisely controlled with a Julabo ME (v.2) recirculating control system containing a mixture of ethylene glycol and water. Prior to experiments, SIFSIX-22-Zn, TIFSIX-6-Zn, GEFSIX-4-Zn, SNFSIX-2-Zn, ZRFSIX-3-Zn, and TAFSEVEN-1-Zn were activated on a Smart VacPrep using dynamic vacuum and heating for 24 h at 333 K.

## RESULTS AND DISCUSSION

**Structural Description.** TIFSIX-6-Zn crystallized in the centrosymmetric orthorhombic space group *Pmma*, SIFSIX-22-Zn, GEFSIX-4-Zn, SNFSIX-2-Zn, and TAFSEVEN-1-Zn crystallized in the centrosymmetric orthorhombic space group *Cmma* while ZRFSIX-3-Zn crystallized in the centrosymmetric orthorhombic space group *Pmmm*. All six structures are comprised as expected: octahedral Zn<sup>2+</sup> ions coordinated to four pyridyl moieties of **tepb** ligands in their equatorial positions and bridging MF<sub>6</sub><sup>2-</sup> (M = Si(IV), Ti(IV), Ge(IV), Sn(IV), and Zr(IV)) or TaF<sub>7</sub><sup>2-</sup> anions in their axial positions. The Zn<sup>2+</sup> ions and **tepb** ligands formed two-dimensional layers pillared by the MF<sub>6</sub><sup>2-</sup> or TaF<sub>7</sub><sup>2-</sup> anions to generate three-dimensional 4,6-connected **fsc** topology networks (Figure 1).

The Zn–F distance in TAFSEVEN-1-Zn is 2.040(2) Å, which lies within the lower quintile (2.061 Å) of the mean distance of 2.108 Å (st. dev. = 0.059 Å) as per the Cambridge Structural Database<sup>39</sup> (CSD, v. 5.41 + 3 updates, see the SI for search parameters), while the Zn–F distances for SIFSIX-22-Zn, TIFSIX-6-Zn, GEFSIX-4-Zn, SNFSIX-2-Zn, and ZRFSIX-3-Zn lie in the second quintile (2.092 Å). The TAFSEVEN-1-Zn Zn–N distance range of 2.176(3) Å lies within the upper quintile (2.157 Å) of the mean distance of 2.138 Å (st. dev. = 0.020 Å) as per the same search query. Zn–N distances for GEFSIX-4-Zn and SNFSIX-2-Zn lie in the third quintile (2.145 Å) while the Zn–N distances for SIFSIX-22-Zn, TIFSIX-6-Zn, and ZRFSIX-3-Zn lie in the fourth quintile (2.157 Å).

The pyridine rings of the **tepb** ligand adopt a propeller-type arrangement about the central benzene ring with rings *para* to each other being co-planar in TIFSIX-6-Zn, GEFSIX-4-Zn,

SNFSIX-2-Zn, ZRFSIX-3-Zn, and TAFSEVEN-1-Zn (Figure 2). The torsion angles of the pyridine ring about the Zn<sup>2+</sup> ions are given in Figures S1–S4 and range from 52.3(2)° to 70.11(5)°. The pyridyl rings are arranged in a propeller-like conformation about the zinc(II) ion. The two-dimensional Zn<sup>2+</sup>-**tepb** layers are pillared by the MF<sub>6</sub><sup>2-</sup> and TaF<sub>7</sub><sup>2-</sup> pillars such that the central aromatic rings of the **tepb** ligands are eclipsed and coplanar when viewed down the crystallographic *a*-axis for SIFSIX-22-Zn, GEFSIX-4-Zn, SNFSIX-2-Zn, ZRFSIX-3-Zn, and TAFSEVEN-1-Zn and the crystallographic *b*-axis for TIFSIX-6-Zn. In the case of TIFSIX-6-Zn and ZRFSIX-3-Zn, the fluorine atoms are modeled as disordered over two positions with each position being eclipsed with the fluorine atoms above and below the plane. For SIFSIX-22-Zn, GEFSIX-4-Zn, SNFSIX-2-Zn, and TAFSEVEN-1-Zn, the equatorial fluorine atoms of the MF<sub>6</sub><sup>2-</sup> pillar are not eclipsed with GEFSIX-4-Zn having the largest pillar rotation angle of 55.0(2)°. In the case of SNFSIX-2-Zn, the equatorial fluorine atoms of the SnF<sub>6</sub><sup>2-</sup> pillar are modeled as disordered over two positions with each position exhibiting noticeably different pillar rotation angles: 4.9(5)° and 23.0(5)°. In the two-dimensional zinc(II)-**tepb** layers, there are two distinct windows (Figure S6), the sizes of which are roughly consistent across all six compounds as the window geometry is independent of the anionic pillar: narrow, square windows where the pyridyl rings are *ortho* relative to one another; larger rectangular windows when pyridyl rings are *meta* relative to one another.

Pore structures were calculated from the crystallographic data of SIFSIX-22-Zn, TIFSIX-6-Zn, GEFSIX-4-Zn, SNFSIX-2-Zn, ZRFSIX-3-Zn, and TAFSEVEN-1-Zn (Poreblazer v4.0, Tables S7, S8). The pore volume per formula unit ranges from 90.49 Å<sup>3</sup> for TAFSEVEN-1-Zn to 135.20 Å<sup>3</sup> for ZRFSIX-3-Zn. The maximum pore diameters vary from 4.71 to 5.92 Å (Poreblazer v4.0), whereas the limiting pore diameters range from 3.18 to 3.72 Å.<sup>40</sup> The constricted pore region is a result of the narrow pore windows occurring in the Zn<sup>2+</sup>-**tepb** layers while the larger pore cavity exists between these two-dimensional layers. This degree of pore constriction is high compared to other HCNs such as **mno** topology networks and

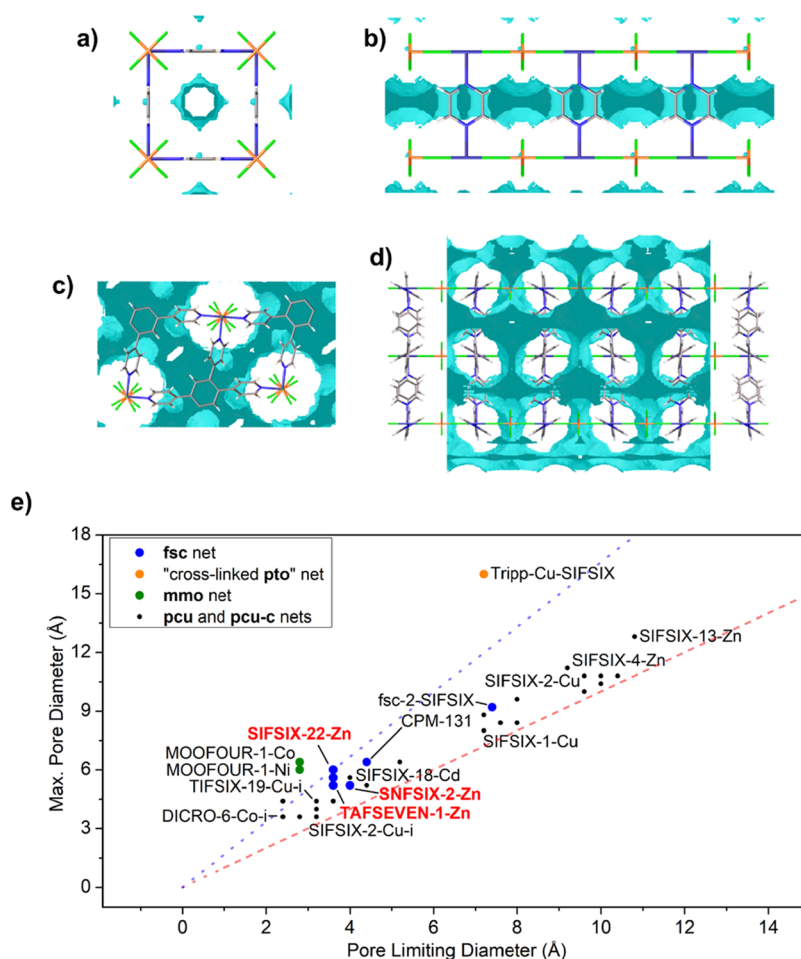


**Figure 3.** Accessible void surface calculated for SIFSIX-3-Zn viewed along the crystallographic (a) *a*- and (b) *c*-directions. Representations of the accessible void surface calculated for SIFSIX-22-Zn viewed along the crystallographic (c) *a*- and (d) *c*-directions. (e) Plot of crystallographically determined maximum and limiting pore diameters in representative HCN materials (red dashed line: idealized cylindrical pores; blue dashed line: the ratio of maximum pore diameter to pore limiting diameter in SIFSIX-22-Zn; see the SI for tabulation).

Tripp-Cu-SIFSIX despite their unique network architectures.<sup>23,29</sup> The highly constricted pores present in SIFSIX-22-Zn, TIFSIX-6-Zn, GEFSIX-4-Zn, SNFSIX-2-Zn, ZRFSIX-3-Zn, and TAFSEVEN-1-Zn are comparable to SIFSIX-18-M and DICRO-6-Co-i among the *pcu* topology HCNs which feature constricted pore environments (Figure 3). For both of the aforementioned materials, the pore constriction arises from the distortion of the one-dimensional metal-pillar-metal chain from a linear to zig-zag arrangement. In SIFSIX-18-M, this is due to the shape of the ligand, whereas in DICRO-6-Co-i it results from the nonlinear geometry of the pillar.<sup>13,41</sup> In contrast, the constriction of pores in SIFSIX-22-Zn, TIFSIX-6-Zn, GEFSIX-4-Zn, SNFSIX-2-Zn, ZRFSIX-3-Zn, and TAFSEVEN-1-Zn arises solely from the dimensions of the Zn<sup>2+</sup>-*tepb* layers.

**Characterization.** Bulk samples of each compound were synthesized by room-temperature slurry methods and characterized by PXRD and TGA (Figures S9–S14). PXRD patterns collected after immersion under MeOH for 1 week revealed that all samples had retained their crystal structures. PXRD patterns collected after exposure to accelerated stability test conditions at 75% R.H. and 40 °C after 1 day and 1 week revealed that SIFSIX-22-Zn underwent hydrolysis and an associated phase change within 1 day, while GEFSIX-4-Zn underwent a phase change between 1 day and 1 week. No

change was observed in the PXRD patterns of TIFSIX-6-Zn, SNFSIX-2-Zn, ZRFSIX-3-Zn, and TAFSEVEN-1-Zn after 1 week, indicating that these pillars provide enhanced hydrolytic stability.

**Gas Sorption.** After activating as-synthesized bulk samples of each HUM, CO<sub>2</sub> sorption isotherms were measured at 195 K to determine their textural characteristics. In all six materials, type I isotherms with steep uptake at low pressure were observed with saturation uptakes of 150–200 cm<sup>3</sup> g<sup>-1</sup> (Figure 4a). Brunauer–Emmett–Teller (BET) surface areas of 387.2, 396.8, 700.0, 615.4, 625.9, and 627.5 m<sup>2</sup> g<sup>-1</sup> were determined for SIFSIX-22-Zn, TIFSIX-6-Zn, GEFSIX-4-Zn, SNFSIX-2-Zn, ZRFSIX-3-Zn, and TAFSEVEN-1-Zn, respectively. The Horvath–Kawazoe plots obtained from 195 K CO<sub>2</sub> data revealed a narrow range of maximum pore widths between 3.7 and 4.1 Å (Figure 4b). These values experimentally confirm the categorization of these materials as ultramicroporous and lie within the range of crystallographically determined pore dimensions (Tables S7–S9). N<sub>2</sub> sorption isotherms were also collected and afforded BET surface area values of 414.3, 478.1, 925.1, 798.1, 1062.0, and 652.9 m<sup>2</sup> g<sup>-1</sup> for SIFSIX-22-Zn, TIFSIX-6-Zn, GEFSIX-4-Zn, SNFSIX-2-Zn, ZRFSIX-3-Zn, and TAFSEVEN-1-Zn, respectively (Figures S16–S21). The variations between saturation CO<sub>2</sub> and N<sub>2</sub> uptakes are attributed to the differing sizes and quadrupole moments of

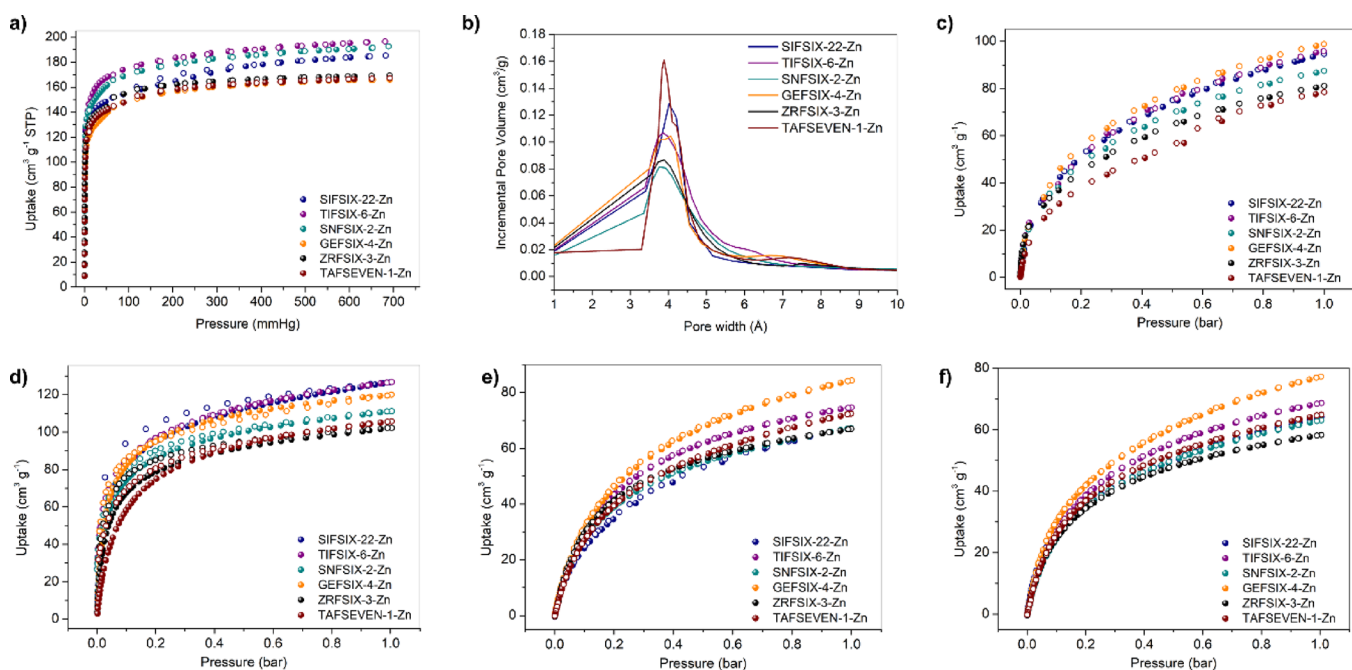


**Figure 4.** (a) 195 K CO<sub>2</sub> sorption isotherms on SIFSIX-22-Zn, TIFSIX-6-Zn, GEFSIX-4-Zn, SNFSIX-2-Zn, ZRFSIX-3-Zn, and TAFSEVEN-1-Zn; (b) Horvath–Kawazoe pore-size distribution plots obtained using 195 K CO<sub>2</sub> isotherms. 298 K sorption isotherms of (c) CO<sub>2</sub>, (d) C<sub>2</sub>H<sub>2</sub>, (e) C<sub>2</sub>H<sub>4</sub>, and (f) C<sub>2</sub>H<sub>6</sub> on SIFSIX-22-Zn, TIFSIX-6-Zn, GEFSIX-4-Zn, SNFSIX-2-Zn, ZRFSIX-3-Zn, and TAFSEVEN-1-Zn.

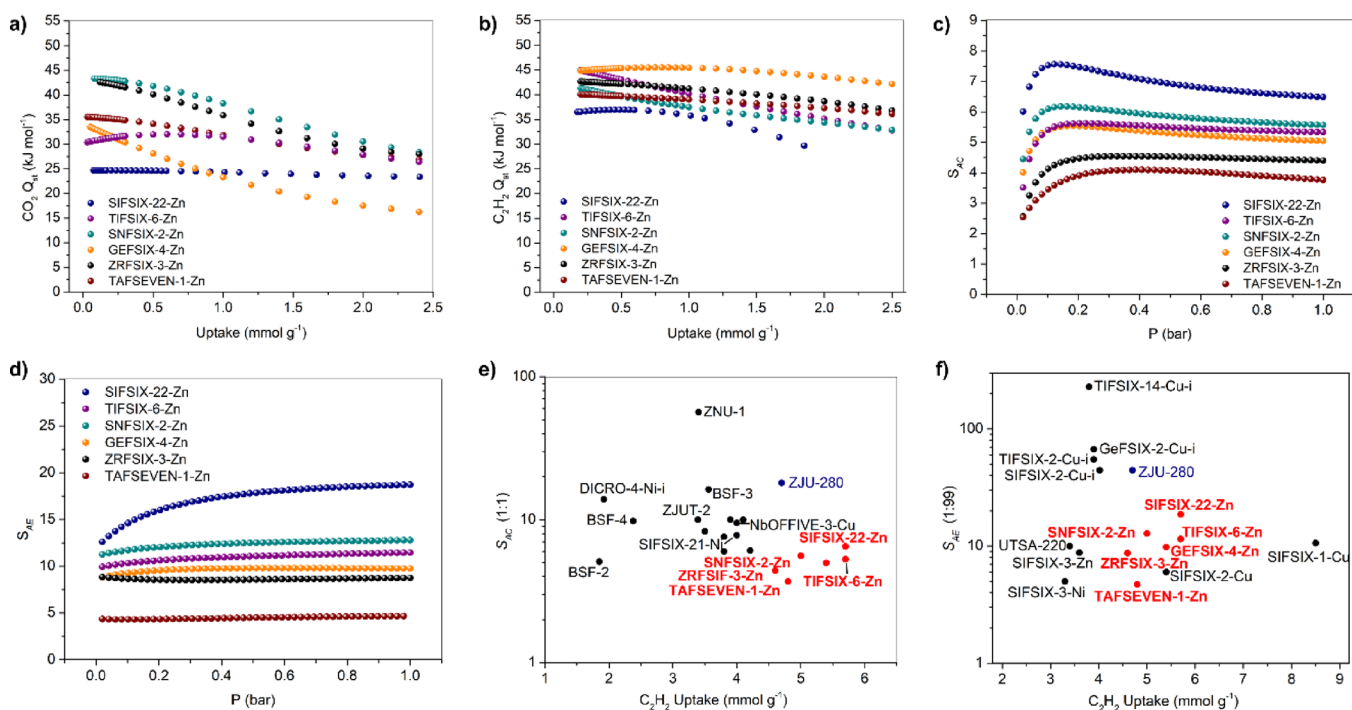


**Figure 5.** Isothermic heats of adsorption of (a) CO<sub>2</sub> and (b) C<sub>2</sub>H<sub>2</sub> on SIFSIX-22-Zn, TIFSIX-6-Zn, GEFSIX-4-Zn, SNFSIX-2-Zn, ZRFSIX-3-Zn, and TAFSEVEN-1-Zn. Ideal adsorbed solution theory (IAST) selectivity determined for (c) 1:1 C<sub>2</sub>H<sub>2</sub>/CO<sub>2</sub> (S<sub>AC</sub>) and (d) 1:99 C<sub>2</sub>H<sub>2</sub>/C<sub>2</sub>H<sub>4</sub> (S<sub>AE</sub>) for SIFSIX-22-Zn, TIFSIX-6-Zn, GEFSIX-4-Zn, SNFSIX-2-Zn, ZRFSIX-3-Zn, and TAFSEVEN-1-Zn. Comparative plots of leading HCNs with respect to (e) S<sub>AC</sub> and (f) S<sub>AE</sub> versus C<sub>2</sub>H<sub>2</sub> uptake.

N<sub>2</sub> and CO<sub>2</sub> and their interactions with the differing electrostatics of the surfaces of each adsorbent.<sup>42</sup>

Following these observations, we investigated the room-temperature sorption properties of each HUM toward CO<sub>2</sub> and C<sub>2</sub> hydrocarbons. The CO<sub>2</sub>, C<sub>2</sub>H<sub>2</sub>, C<sub>2</sub>H<sub>4</sub>, and C<sub>2</sub>H<sub>6</sub> sorption isotherms for SIFSIX-22-Zn, TIFSIX-6-Zn, GEF-

SIX-4-Zn, SNFSIX-2-Zn, and ZRFSIX-3-Zn are well-defined Langmuir-type profiles (Figure 4c–f). PXRD data collected after sorption experiments support the apparent reversibility of the isotherms and no loss of crystallinity was observed (Figures S9–S14). CO<sub>2</sub> uptakes at 298 K varied from a maximum of 99 cm<sup>3</sup> g<sup>-1</sup> in GEFSIX-4-Zn to a minimum of 81 cm<sup>3</sup> g<sup>-1</sup> in

**ZRFSIX-3-Zn.** Similarly, 298 K C<sub>2</sub>H<sub>2</sub> uptakes ranged from 127 cm<sup>3</sup> g<sup>-1</sup> in **TIFSIX-6-Zn** to 102 cm<sup>3</sup> g<sup>-1</sup> in **ZRFSIX-3-Zn**. C<sub>2</sub>H<sub>4</sub> and C<sub>2</sub>H<sub>6</sub> isotherms exhibited similar profiles, with lower uptakes overall vs. C<sub>2</sub>H<sub>2</sub>. The only deviation from ideal Langmuir-type profiles was seen in the CO<sub>2</sub> isotherm of **TAFSEVEN-1-Zn**, in which a minor inflection occurred at ca. 0.55 bar and 298 K. We attribute this anomaly to the five equatorial fluorides in the TaF<sub>7</sub><sup>2-</sup> pillar leading to a distinct electrostatic distribution vs MF<sub>6</sub><sup>2-</sup> pillars, thereby impacting sorption through F...H<sub>Ar</sub> contacts to the **tepb** ligands by altering ligand conformation and pore dimensions.

Isothermic heats of sorption (Q<sub>st</sub>) were calculated for CO<sub>2</sub> and C<sub>2</sub> gases for all six adsorbents (Figure 5a,b). Low loading Q<sub>st</sub> values for CO<sub>2</sub> varied from 43.3 and 42.6 kJ mol<sup>-1</sup> for **SNFSIX-2-Zn** and **ZRFSIX-3-Zn**, respectively, to 30.4 and 24.7 kJ mol<sup>-1</sup> for **TIFSIX-6-Zn** and **SIFSIX-22-Zn**, respectively. Low loading Q<sub>st</sub> values for C<sub>2</sub>H<sub>2</sub> were determined to be relatively higher with a narrower range, from 44.8 kJ mol<sup>-1</sup> for **TIFSIX-6-Zn** and **GEFSIX-4-Zn** to 36.5 kJ mol<sup>-1</sup> for **SIFSIX-22-Zn**. In contrast, Q<sub>st</sub> values for C<sub>2</sub>H<sub>4</sub> and C<sub>2</sub>H<sub>6</sub> range from 33.3 to 31.6 kJ mol<sup>-1</sup> for C<sub>2</sub>H<sub>4</sub> and 32.7 to 31.1 kJ mol<sup>-1</sup> for C<sub>2</sub>H<sub>6</sub> (Figures S22, S23). Overall, the affinity for C<sub>2</sub>H<sub>2</sub> was highest, encouraging us to evaluate the selectivity of the six HUMs in the context of C<sub>2</sub>H<sub>2</sub>/CO<sub>2</sub> and C<sub>2</sub>H<sub>2</sub>/C<sub>2</sub>H<sub>4</sub> separations.

Calculations conducted using ideal adsorbed solution theory (IAST) indicate that C<sub>2</sub>H<sub>2</sub>/CO<sub>2</sub> (1:1) selectivities (S<sub>AC</sub>) vary between 6.5 (**SIFSIX-22-Zn**) and 3.8 (**TAFSEVEN-1-Zn**) at 1 bar. C<sub>2</sub>H<sub>2</sub>/C<sub>2</sub>H<sub>4</sub> (1:99) selectivities (S<sub>AE</sub>) at 1 bar vary between 18.7 (**SIFSIX-22-Zn**) and 4.7 (**TAFSEVEN-1-Zn**) (Figure 5c,d). Perhaps most notable is that, despite the absence of any apparent correlation between pure component Q<sub>st</sub> values for adsorbents and different gases, S<sub>AC</sub> and S<sub>AE</sub> values follow a clear trend, that is, **SIFSIX-22-Zn** > **SNFSIX-2-Zn** > **TIFSIX-6-Zn** > **GEFSIX-4-Zn** > **ZRFSIX-3-Zn** > **TAFSEVEN-1-Zn**. This correlation suggests that the identity of inorganic anions is responsible for the varying affinity toward acetylene in these HUMs and that the sorption properties are impacted by incorporation of different pillars. No correlation between S<sub>AC</sub> and S<sub>AE</sub> values with the electronegativity of the central atom of the anion was evident, suggesting a need for calculation of pore surface charges and in-depth detailed computational studies on this system to fully elucidate the observed affinities toward C<sub>2</sub>H<sub>2</sub>.

The calculated selectivity values of these adsorbents are moderate but when viewed together with their relatively high uptakes, it is apparent that these **fsc** networks address the trade-off between selectivity and uptake (Figure 5e,f). When compared to other C<sub>2</sub>H<sub>2</sub> selective sorbents, **SIFSIX-22-Zn** and **TIFSIX-6-Zn** show a rare combination of strong selectivity and high uptake, indicating that further exploration of this platform of materials has the potential to produce adsorbents with strong overall performance.

## CONCLUSIONS

We report herein the highly modular **fsc** topology HUM platform which enabled us to explore the effect of changing inorganic pillar on gas sorption properties. The use of SiF<sub>6</sub><sup>2-</sup>, TiF<sub>6</sub><sup>2-</sup>, GeF<sub>6</sub><sup>2-</sup>, SnF<sub>6</sub><sup>2-</sup>, ZrF<sub>6</sub><sup>2-</sup>, and TaF<sub>7</sub><sup>2-</sup> in combination with Zn<sup>2+</sup> and the tetratopic **tepb** ligand afforded a family of HUMs: **SIFSIX-22-Zn**, **TIFSIX-6-Zn**, **GEFSIX-4-Zn**, **SNFSIX-2-Zn**, and **ZRFSIX-3-Zn** and the first TaF<sub>7</sub><sup>2-</sup>-pillared HUM, **TAFSEVEN-1-Zn**. The crystal structures were

determined by single-crystal X-ray diffraction and enabled systematic studies of structure–property relationships. Each framework features narrow pore windows, yet significant pore cavities between the zinc(II)-**tepb** layers. This is unusual in HUMs and presents a general strategy that could address the trade-off between uptake and selectivity that is common in adsorbents. Variation of the inorganic pillar resulted in a trend in relative C<sub>2</sub>H<sub>2</sub> affinity as follows: **SIFSIX-22-Zn** > **SNFSIX-2-Zn** > **TIFSIX-6-Zn** > **GEFSIX-4-Zn** > **ZRFSIX-3-Zn** > **TAFSEVEN-1-Zn**. Overall, this work highlights the modular nature of the **fsc** HUM platform and that substitution of the inorganic pillar impacts structure–property relationships.

## ASSOCIATED CONTENT

### Supporting Information

The Supporting Information is available free of charge at <https://pubs.acs.org/doi/10.1021/acs.cgd.2c00561>.

Single-crystal X-ray diffraction data, powder X-ray diffraction patterns, thermal gravimetric analyses, pore analyses, gas sorption isotherms, and IAST calculations for all materials (PDF)

### Accession Codes

CCDC 2151309–2151313 contain the supplementary crystallographic data for this paper. These data can be obtained free of charge via [www.ccdc.cam.ac.uk/data\\_request/cif](http://www.ccdc.cam.ac.uk/data_request/cif), or by emailing [data\\_request@ccdc.cam.ac.uk](mailto:data_request@ccdc.cam.ac.uk), or by contacting The Cambridge Crystallographic Data Centre, 12 Union Road, Cambridge CB2 1EZ, UK; fax: +44 1223 336033.

## AUTHOR INFORMATION

### Corresponding Author

Michael J. Zaworotko – Department of Chemical Sciences, Bernal Institute, University of Limerick, Limerick V94 T9PX, Republic of Ireland; [orcid.org/0000-0002-1360-540X](https://orcid.org/0000-0002-1360-540X); Email: [xtal@ul.ie](mailto:xtal@ul.ie)

### Authors

Debobroto Sensharma – Department of Chemical Sciences, Bernal Institute, University of Limerick, Limerick V94 T9PX, Republic of Ireland; [orcid.org/0000-0002-4918-0730](https://orcid.org/0000-0002-4918-0730)

Benjamin H. Wilson – Department of Chemical Sciences, Bernal Institute, University of Limerick, Limerick V94 T9PX, Republic of Ireland

Naveen Kumar – Department of Chemical Sciences, Bernal Institute, University of Limerick, Limerick V94 T9PX, Republic of Ireland

Daniel J. O'Hearn – Department of Chemical Sciences, Bernal Institute, University of Limerick, Limerick V94 T9PX, Republic of Ireland

Complete contact information is available at: <https://pubs.acs.org/10.1021/acs.cgd.2c00561>

### Author Contributions

#D.S. and B.H.W. contributed equally. The manuscript was written through contributions of all authors. All authors have given approval to the final version of the manuscript.

### Funding

M.J.Z. acknowledges funding from Science Foundation Ireland (16/IA/4624) and the European Research Council (ADG 885695).

### Notes

The authors declare no competing financial interest.

## ■ ABBREVIATIONS

SCXRD, single crystal X-ray diffraction; PXRD, powder X-ray diffraction; TGA, thermal gravimetric analysis; tepb, 1,2,4,5-tetra(4-pyridyl)benzene.; IAST, ideal adsorbed solution theory

## ■ REFERENCES

- (1) Subramanian, S.; Zaworotko, M. J. Porous solids by design:  $[\text{Zn}(4, 4'\text{-bpy})_2(\text{SiF}_6)] \cdot n \cdot x\text{DMF}$ , a single framework octahedral coordination polymer with large square channels. *Angew. Chem., Int. Ed.* **1995**, *34*, 2127–2129.
- (2) O'Hearn, D. J.; Bajpai, A.; Zaworotko, M. J. The "Chemistree" of Porous Coordination Networks: Taxonomic Classification of Porous Solids to Guide Crystal Engineering Studies. *Small* **2021**, *17*, No. 2006351.
- (3) Mukherjee, S.; Zaworotko, M. J. Crystal engineering of hybrid coordination networks: from form to function. *Trends Chem.* **2020**, *2*, 506–518.
- (4) Nugent, P.; Belmabkhout, Y.; Burd, S. D.; Cairns, A. J.; Luebke, R.; Forrest, K.; Pham, T.; Ma, S.; Space, B.; Wojtas, L.; Eddaoudi, M.; Zaworotko, M. J. Porous materials with optimal adsorption thermodynamics and kinetics for CO<sub>2</sub> separation. *Nature* **2013**, *495*, 80–84.
- (5) Burd, S. D.; Ma, S.; Perman, J. A.; Sikora, B. J.; Snurr, R. Q.; Thallapally, P. K.; Tian, J.; Wojtas, L.; Zaworotko, M. J. Highly selective carbon dioxide uptake by  $[\text{Cu}(\text{bpy}-n)_2(\text{SiF}_6)]$  (bpy-1= 4, 4'-bipyridine; bpy-2= 1, 2-bis(4-pyridyl) ethene). *J. Am. Chem. Soc.* **2012**, *134*, 3663–3666.
- (6) Zhang, Z.; Cui, X.; Yang, L.; Cui, J.; Bao, Z.; Yang, Q.; Xing, H. Hexafluorogermanate (GeFSIX) anion-functionalized hybrid ultramicroporous materials for efficiently trapping acetylene from ethylene. *Ind. Eng. Chem. Res.* **2018**, *57*, 7266–7274.
- (7) Bajpai, A.; Lusi, M.; Zaworotko, M. J. The role of weak interactions in controlling the mode of interpenetration in hybrid ultramicroporous materials. *Chem. Commun.* **2017**, *53*, 3978–3981.
- (8) Liu, J.-J.; Hong, Y.-J.; Guan, Y.-F.; Lin, M.-J.; Huang, C.-C.; Dai, W.-X. Lone pair- $\pi$  interaction-induced generation of non-interpenetrated and photochromic cuboid 3-D naphthalene diimide coordination networks. *Dalton Trans.* **2015**, *44*, 653–658.
- (9) Cadiau, A.; Belmabkhout, Y.; Adil, K.; Bhatt, P. M.; Pillai, R. S.; Shkurenko, A.; Martineau-Corcoss, C.; Maurin, G.; Eddaoudi, M. Hydrolytically stable fluorinated metal-organic frameworks for energy-efficient dehydration. *Science* **2017**, *356*, 731–735.
- (10) Lin, M.-J.; Jouaiti, A.; Kyritsakas, N.; Hosseini, M. W. Molecular tectonics: modulation of size and shape of cuboid 3-D coordination networks. *CrystEngComm* **2009**, *11*, 189–191.
- (11) Zhang, Z.; Yang, Q.; Cui, X.; Yang, L.; Bao, Z.; Ren, Q.; Xing, H. Sorting of C<sub>4</sub> olefins with interpenetrated hybrid ultramicroporous materials by combining molecular recognition and size-sieving. *Angew. Chem., Int. Ed.* **2017**, *56*, 16282–16287.
- (12) Kumar, A.; Madden, D. G.; Lusi, M.; Chen, K. J.; Daniels, E. A.; Curtin, T.; Perry, J. J., IV; Zaworotko, M. J. Direct air capture of CO<sub>2</sub> by physisorbent materials. *Angew. Chem., Int. Ed.* **2015**, *54*, 14372–14377.
- (13) Mukherjee, S.; Sikdar, N.; O'Nolan, D.; Franz, D. M.; Gascón, V.; Kumar, A.; Kumar, N.; Scott, H. S.; Madden, D. G.; Kruger, P. E.; Space, B.; Zaworotko, M. J. Trace CO<sub>2</sub> capture by an ultramicroporous physisorbent with low water affinity. *Sci. Adv.* **2019**, *5*, No. eaax9171.
- (14) Mohamed, M. H.; Elsaidi, S. K.; Pham, T.; Forrest, K. A.; Schaeff, H. T.; Hogan, A.; Wojtas, L.; Xu, W.; Space, B.; Zaworotko, M. J.; Thallapally, P. K. Hybrid Ultra-Microporous Materials for Selective Xenon Adsorption and Separation. *Angew. Chem., Int. Ed.* **2016**, *55*, 8285–8289.
- (15) Bhatt, P. M.; Belmabkhout, Y.; Cadiau, A.; Adil, K.; Shekhah, O.; Shkurenko, A.; Barbour, L. J.; Eddaoudi, M. A fine-tuned fluorinated MOF addresses the needs for trace CO<sub>2</sub> removal and air capture using physisorption. *J. Am. Chem. Soc.* **2016**, *138*, 9301–9307.
- (16) Kumar, A.; Hua, C.; Madden, D. G.; O'Nolan, D.; Chen, K.-J.; Keane, L.-A. J.; Perry, J. J.; Zaworotko, M. J. Hybrid ultramicroporous materials (HUMs) with enhanced stability and trace carbon capture performance. *Chem. Commun.* **2017**, *53*, 5946–5949.
- (17) Scott, H. S.; Bajpai, A.; Chen, K.-J.; Pham, T.; Space, B.; Perry, J. J.; Zaworotko, M. J. Novel mode of 2-fold interpenetration observed in a primitive cubic network of formula  $[\text{Ni}(1,2\text{-bis}(4\text{-pyridyl})\text{-acetylene})_2(\text{Cr}_2\text{O}_7)]_n$ . *Chem. Commun.* **2015**, *51*, 14832–14835.
- (18) Scott, H. S.; Ogiwara, N.; Chen, K.-J.; Madden, D. G.; Pham, T.; Forrest, K.; Space, B.; Horike, S.; Perry, J. J., IV; Kitagawa, S. Crystal engineering of a family of hybrid ultramicroporous materials based upon interpenetration and dichromate linkers. *Chem. Sci.* **2016**, *7*, 5470–5476.
- (19) Scott, H. S.; Shivanna, M.; Bajpai, A.; Chen, K.-J.; Madden, D. G.; Perry, J. J., IV; Zaworotko, M. J. Enhanced Stability toward Humidity in a Family of Hybrid Ultramicroporous Materials Incorporating Cr<sub>2</sub>O<sub>7</sub><sup>2-</sup> Pillars. *Cryst. Growth Des.* **2017**, *17*, 1933–1937.
- (20) Li, B.; Cui, X.; O'Nolan, D.; Wen, H. M.; Jiang, M.; Krishna, R.; Wu, H.; Lin, R. B.; Chen, Y. S.; Yuan, D.; Zhou, W.; Ren, Q.; Qian, G.; Zaworotko, M. J.; Chen, B. An ideal molecular sieve for acetylene removal from ethylene with record selectivity and productivity. *Adv. Mater.* **2017**, *29*, No. 1704210.
- (21) Lin, R.-B.; Xiang, S.; Zhou, W.; Chen, B. Microporous metal-organic framework materials for gas separation. *Chem* **2020**, *6*, 337–363.
- (22) Yang, L.; Cui, X.; Yang, Q.; Qian, S.; Wu, H.; Bao, Z.; Zhang, Z.; Ren, Q.; Zhou, W.; Chen, B. A single-molecule propyne trap: highly efficient removal of propyne from propylene with anion-pillared ultramicroporous materials. *Adv. Mater.* **2018**, *30*, No. 1705374.
- (23) Mohamed, M. H.; Elsaidi, S. K.; Wojtas, L.; Pham, T.; Forrest, K. A.; Tudor, B.; Space, B.; Zaworotko, M. J. Highly selective CO<sub>2</sub> uptake in uninodal 6-connected "mmo" nets based upon MO<sub>4</sub><sup>2-</sup> (M = Cr, Mo) pillars. *J. Am. Chem. Soc.* **2012**, *134*, 19556–19559.
- (24) Qian, Q.-L.; Gu, X.-W.; Pei, J.; Wen, H.-M.; Wu, H.; Zhou, W.; Li, B.; Qian, G. A novel anion-pillared metal-organic framework for highly efficient separation of acetylene from ethylene and carbon dioxide. *J. Mater. Chem. A* **2021**, *9*, 9248–9255.
- (25) Lin, Q.; Mao, C.; Kong, A.; Bu, X.; Zhao, X.; Feng, P. Porphyrinic coordination lattices with fluoropillars. *J. Mater. Chem. A* **2017**, *5*, 21189–21195.
- (26) He, L.; Nath, J. K.; Lin, Q. Robust multivariate metal-porphyrin frameworks for efficient ambient fixation of CO<sub>2</sub> to cyclic carbonates. *Chem. Commun.* **2019**, *55*, 412–415.
- (27) Liu, Y.; Zhang, Y.; Zhang, P.; Peng, Y.; Liu, X.; Chen, J.; Chen, S.; Zeng, Z.; Wang, J.; Deng, S. Two novel 4, 6-connected anion-pillared metal-organic frameworks for simultaneous separation of C<sub>3</sub> and C<sub>4</sub> olefins. *Chem. Eng. Process.: Process Intensif.* **2022**, *172*, No. 108768.
- (28) Elsaidi, S. K.; Mohamed, M. H.; Pham, T.; Hussein, T.; Wojtas, L.; Zaworotko, M. J.; Space, B. Crystal engineering of a 4,6-c fsc platform that can serve as a carbon dioxide single-molecule trap. *Cryst. Growth Des.* **2016**, *16*, 1071–1080.
- (29) Lusi, M.; Fecine, P. B.; Chen, K.-J.; Perry, J. J.; Zaworotko, M. J. A rare cationic building block that generates a new type of polyhedral network with "cross-linked" pto topology. *Chem. Commun.* **2016**, *52*, 4160–4162.
- (30) Li, H.; Liu, C.; Chen, C.; Di, Z.; Yuan, D.; Pang, J.; Wei, W.; Wu, M.; Hong, M. An Unprecedented Pillar-Cage Fluorinated Hybrid Porous Framework with Highly Efficient Acetylene Storage and Separation. *Angew. Chem., Int. Ed.* **2021**, *60*, 7547–7552.
- (31) Sensharma, D.; O'Hearn, D. J.; Koochaki, A.; Bezrukov, A. A.; Kumar, N.; Wilson, B. H.; Vandichel, M.; Zaworotko, M. J. The first sulfate-pillared hybrid ultramicroporous material, SOFOUR-1-Zn, and its acetylene capture properties. *Angew. Chem., Int. Ed.* **2022**, *61*, No. e202116145.

- (32) Chang, Y.-C.; Wang, S.-L. From stimuli-responsive poly-morphic organic dye crystals to photoluminescent cationic open-framework metal phosphate. *J. Am. Chem. Soc.* **2012**, *134*, 9848–9851.
- (33) Bruker, APEX3, SaS; Bruker AXS Inc.: Madison, WI, 2015.
- (34) Sheldrick, G. SADABS; University of Göttingen: Göttingen, Germany, 1996.
- (35) Sheldrick, G. M. SHELXT—Integrated space-group and crystal-structure determination. *Acta Crystallogr., A* **2015**, *71*, 3–8.
- (36) Sheldrick, G. M. Crystal structure refinement with SHELXL. *Acta Crystallogr., C* **2015**, *71*, 3–8.
- (37) Dolomanov, O. V.; Bourhis, L. J.; Gildea, R. J.; Howard, J. A.; Puschmann, H. OLEX2: a complete structure solution, refinement and analysis program. *J. Appl. Crystallogr.* **2009**, *42*, 339–341.
- (38) Spek, A. L. PLATON SQUEEZE: a tool for the calculation of the disordered solvent contribution to the calculated structure factors. *Acta Crystallogr., C* **2015**, *71*, 9–18.
- (39) Groom, C. R.; Bruno, I. J.; Lightfoot, M. P.; Ward, S. C. The Cambridge structural database. *Acta Crystallogr., B* **2016**, *72*, 171–179.
- (40) Sarkisov, L.; Harrison, A. Computational structure characterisation tools in application to ordered and disordered porous materials. *Mol. Simul.* **2011**, *37*, 1248–1257.
- (41) Ponomarova, V. V.; Komarchuk, V. V.; Boldog, I.; Krautscheid, H.; Domasevitch, K. V. Modular construction of 3D coordination frameworks incorporating  $\text{SiF}_6^{2-}$  links: Accessing the significance of  $[\text{M}(\text{pyrazole})_4(\text{SiF}_6)]$  synthon. *CrystEngComm* **2013**, *15*, 8280–8287.
- (42) Islamoglu, T.; Idrees, K. B.; Son, F. A.; Chen, Z.; Lee, S. J.; Li, P.; Farha, O. K. Are you using the right probe molecules for assessing the textural properties of metal–organic frameworks? *J. Mater. Chem. A* **2022**, *10*, 157–173.

## Recommended by ACS

### Surface Area and Porosity of $\text{Co}_3(\text{ndc})_3(\text{dabco})$ Metal–Organic Framework and Its Methane Storage Capacity: A Combined Experimental and Simulation...

Rui P. P. L. Ribeiro and José P. B. Mota

JANUARY 25, 2021  
THE JOURNAL OF PHYSICAL CHEMISTRY C

READ 

### Modeling High-Pressure Hydrogen Uptake by Nanoporous Metal–Organic Frameworks: Implications for Hydrogen Storage and Delivery

Pamela Ramirez-Vidal, Vanessa Fierro, *et al.*

JANUARY 10, 2022  
ACS APPLIED NANO MATERIALS

READ 

### In Silico Tuning of the Pore Surface Functionality in Al-MOFs for Trace $\text{CH}_3\text{I}$ Capture

Xiaoyu Wu, Lifeng Ding, *et al.*

JULY 12, 2021  
ACS OMEGA

READ 

### Confinement-Directed Adsorption of Noble Gases (Xe/Kr) in MFM-300(M)-Based Metal–Organic Framework Materials

Srinivasu Kancharlapalli, Tapan K. Ghanty, *et al.*

OCTOBER 22, 2019  
THE JOURNAL OF PHYSICAL CHEMISTRY C

READ 

Get More Suggestions >